2017 IEEE/RSJ International Conference on Intelligent Robots and Systems (IROS)
September 24–28, 2017, Vancouver, BC, Canada

Design and Analysis of a Novel Planar Robotic Leg for High-Speed Locomotion

Vinay R. Kamidi, Wael Saab, and Pinhas Ben-Tzvi, *Senior Member, IEEE*

***Abstract*— This paper presents the mechanical design and analysis of a novel leg mechanism that has only one active degree of freedom (DOF). The proposed mechanism is intended towards simplifying the mechanical and control complexity identified with the robotic legs implemented on quadrupedal platforms capable of dynamic locomotion. First, a survey of high-speed and reduced DOF legged robotic systems is presented to elucidate the design challenges and determine system requirements. Drawing from these requirements, a novel design of a six-bar leg mechanism with a single DOF is proposed. The novelty of the mechanism lies in its ability to trace a path that accommodates the execution of trot-gait by the quadrupedal platform realized by integrating the proposed leg. The kinematics of the mechanism is formulated and a multi-body model is used to perform a series of case studies on the sensitivity of the foot trajectory to the leg's dimensional parameters. Preliminary work on optimization of the foot trajectory is then performed. This research will ultimately assist the future design of quadrupedal robots to test the ability of spatial robotic tails in stabilizing and maneuvering the platform.**

I. Introduction

Legged locomotion has shown potential benefits in traversing uneven terrain and obstacles in comparison to wheeled and tracked vehicles [1]. Only a few robots have been successfully implemented in real-world applications due to relative complexity of design and control of legged machines. Such examples include, but are not limited to, the ANYmal quadruped [2] and the Adaptive Suspension Vehicle [3] developed for nuclear power plant maintenance and field transportation, respectively.

Considerable research was devoted to the investigation of dynamic stability control [4], and walking pattern generation [5]. However, the leg mechanism determines the number of active DOF required for operation. This corresponds to the efficiency of the system, thus making these components fundamental for the design and operational aspects of legged robots as pointed out in [6]. For a legged robot to navigate utilizing a symmetric or asymmetric gait, perform forward motion, and turning maneuvers on uneven terrain, a minimum of three active DOFs are required for spatial positioning. Turning is often the least used motion during walking/trotting gaits. Traditionally the hip Abduction/ Adduction (HAA) DOF is responsible for turning and is separated from the other two-DOFs, hip Extension/Flexion (HFE) and knee Extension/Flexion (KFE). Typically, two DOF leg designs [7] are sufficient to engage HFE and KFE to locomote dynamically in a plane. However, multiple actuators are required to change direction cyclically during a walking/trotting gait. In addition, both DOFs must be controlled simultaneously, which results in complex control algorithms and slow speed, static gaits when implemented either on bipedal/quadrupedal robots.

To address these challenges, the authors present a novel single-DOF leg conducive to performing a dynamic gait, namely trotting/running-trot at high speeds when mounted on a quadrupedal platform. This paper investigates the hypothesis that leg mechanisms designed with reduced DOFs can trace a foot trajectory favorable to dynamic locomotion.

The long-term goal of this research is to develop a quadrupedal robot capable of performing high-speed, planar trot-running. The fully integrated quadruped will be used as an experimental platform to investigate the benefits of stabilization and maneuvering of legged robots using articulated spatial robotic tails [8]–[11].

II. Motivation

A. High-Speed Legged Locomotion

This section reviews high-speed legged robots with emphasis on their design topologies, active DOFs, gait types and the demonstrated forward velocities of the legged robotic platform.

Observations from nature indicate that fast locomotion can be realized by asymmetric gaits such as trotting and bounding [12]. These gaits are referred to as dynamic gaits due to the requirement of active balancing while in motion. The step cycles involved in these motions may be divided into two stages: the stance phase, in which the foot contacts the ground, absorbs impact forces, and pushes the robot forward, and the swing phase, in which the leg is moved to a new contact point.

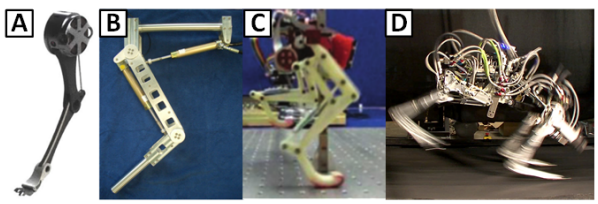

Fig.1. Existing high-speed legged robots: (A) MIT Cheetah [27], (B) HYQ leg [28], (C) KAIST robotic leg [17], (D) Boston Dynamics Cheetah [29].

* This material is based upon work supported by the National Science Foundation under Grant No. 1557312.

V.R. Kamidi, W. Saab, P. Ben-Tzvi are with the Robotics and Mechatronics Lab, Virginia Tech, Blacksburg, VA 24060 USA (email: {vinay28,wael,bentzvi}@vt.edu)

The MIT Cheetah Quadruped, shown in Fig. 1(A), utilizes legs with two active DOFs and custom designed actuators located at the hip and shoulder joints and has demonstrated trotting speeds of 6 m/s [13]. It employs virtual compliance between the hip and the distal link of its three-link leg structure, where a multi-layered controller is used to shield the motors from impact forces [14]. The HYQ, a hydraulically and electrically actuated quadruped, shown in Fig. 1(B), employs legs with three active DOFs each and has exhibited trotting at speeds up to 2.2 m/s [15]. It utilizes a two-link leg similar in structure to that of plantigrades, and employed a high-level controller to plan its leg trajectory [16]. The KAIST robot, illustrated in Fig. 1(C), is a bipedal platform that runs at an average speed of 0.75 m/s, with a step frequency of 2.8 HZ [17]. Its motors are also located at the hip and it uses a physical spring positioned in the distal part of the leg to absorb impact forces experienced at the foot in dynamic locomotion. Fig. 1(D) shows the Boston Dynamics Cheetah, which reported a maximum attainable speed on a treadmill of 12.9 m/s using an off-board hydraulic unit with its digitigrade leg structure.

As the above discussion demonstrates, in platforms employing electric actuation and tetherless locomotion it is preferable to locate motors close to the hip, so that the reflected inertia at the distal part of the legs is reduced, and higher speeds can be achieved. It also worth noting that compliance within the leg mechanism, physical or virtual, is necessary to absorb the impact forces of high-speed locomotion. However, the majority of legs in the literature have to synchronize multiple actuators and employ a multi-layered control structure in order to execute the required trajectory. In addition, the integration of multiple active DOF joints correlate to a greater mass and bulkier structures requiring more power from the motors to locomote.

B. Reduced-Degree of Freedom Leg Designs

To address the challenges of highly articulated leg design, researchers have investigated reduced-DOF strategies. In this paper, a reduced-DOF legged system is defined as one possessing one or two active DOFs. The RMLeg is a two-DOF leg composed of two four-bar mechanisms in an arrangement designed to produce a stable walking gait [7]. The design requires two motors working in tandem to generate one step cycle, resulting in low efficiency, as its reported speed of 0.1 m/s reflects. The Rhex robot utilizes six C-shaped legs, each independently actuated and capable of continuous rotation about a motor shaft [18]. The robot successfully implemented a pronking gait at 0.55 m/s.

A variety of single-DOF leg mechanisms, such as those depicted in Fig. 2, have been explored in previous research [19]. Analysis of reported trajectories shows that these mechanisms produce approximately straight-line stance phase trajectories. The Jansen mechanism depicted in Fig. 2(A), the Ghassei linkage in Fig. 2(B), and the Klann linkage, as shown in Fig. 2(C), are all crank-based leg mechanisms that exhibit straight-line approximations [20]. Many of the trajectories that can be created by the Watt-I mechanism in Fig. 2(D), and the Stephenson-II and Stephenson-III mechanisms in Fig. 2(E) and Fig. 2(F)

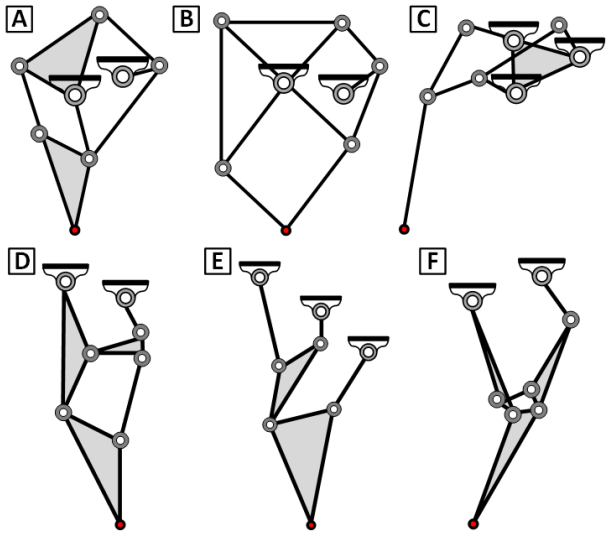

Fig. 2. Formerly studied/implemented single-DOF leg mechanisms: (A) Jansen Linkage, (B) Ghassei linkage, (C) Klann Mechanism, (D) Watt-I, (E) Stephenson-II, (F) Stephenson-III

respectively, have complicated swing phases that require the leg to trace complicated curves or suddenly transition into protraction, resulting in undesirable sharp turns. Prior analysis shows that the stance-phase trajectory for fast locomotion is dictated by the minimum amount of time the leg is in contact with the ground, as is exhibited by the sinusoidal wave observations made in [21].

Simple mechanisms with reduced DOFs may be constructed, which have lower mass, cost, and control requirements than legs with three or more DOFs. The drawback of these designs is that they limit the achievable workspace of the leg, thus making it difficult to maintain stability while executing dynamic gaits or maneuvers. Reduced-DOF legs typically compensate for their reduced workspace by employing static gaits, redundant structures, or lower speed walking gaits. However, reduced-DOF mechanisms must also deal with the problem of motor synchronization. Additionally, running at high speeds is more efficient if actuators are not required to change direction during a step cycle. In summary, while reduced-DOF mechanisms are a promising means of reducing the design and control complexity involved in leg locomotion, the problems of minimizing ground contact, synchronizing motor actuation, and optimizing distal mass distribution in such systems remain a research challenge

C. Design Motivation

It is desirable for a legged robot to have an efficient control structure and a simple mechanical structure while at the same time being capable of locomoting at high-speeds. Furthermore, fast running is a function of both the actuation and the physical characteristics of the leg mechanism. Exploiting the properties of single-DOF mechanisms removes the need for synchronized motor control within the leg. As stated previously, minimization of the distal mass of the mechanism transfers the leg's inertial moment closer to the body, thus increasing achievable speed. In addition, the

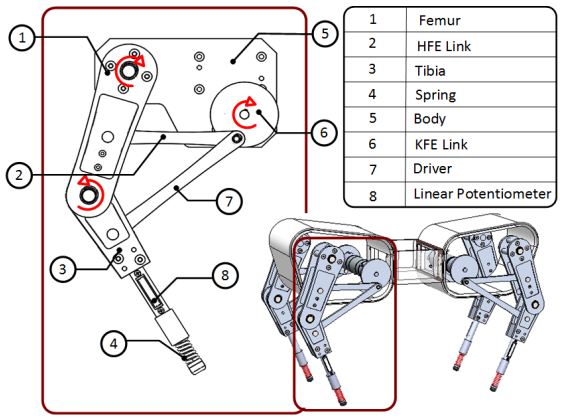

Fig. 3. Schematic diagram of the leg mechanism. A rendering of the quadruped integrated with the novel leg (inset).

trajectory must be smooth in order minimize ground contact, thus increasing the force generated with each step to propel forward. The angle of attack (the angle at which the leg approaches the ground) plays a crucial role in stable running. Therefore, it has to be kept to a minimum as established in.[22] Finally, the desire for a compact and robust mechanism is to reduce the required actuation power while still enabling it to withstand the high impact motion of running. Therefore, the objective of this research is summarized according to the following requirements for the leg to satisfy:

1. The leg mechanism should only be driven by a single, continuously rotating link.
2. The mechanism should be designed with reduced inertia for high-speed applications.
3. The generated foot trajectory should be a smooth closed loop curve.
4. The angle of attack should be minimized.
5. The mechanism should be compact and robust.

III. Mechanical Design

This section details the mechanical design of the proposed leg mechanism, illustrated in a schematic diagram shown in Fig. 3. The leg is a six-bar mechanism, with its five links denoted as the femur, tibia, HFE link, KFE link, and the driver link, responsible for actuation.

The driver is attached to a high power geared motor and is capable of continuous rotation. Motion is transferred to the femur and tibia links via the HFE and KFE linkages resulting in a closed loop, smooth foot trajectory, a sample of which is shown in Fig. 4. This mechanical arrangement fulfills Requirement 1. The hip and the driver are located close to each other on the body, at an offset, with the driver placed close to the hip to satisfy Requirement 2.

In order to dissipate energy resulting from impact during a high-speed gait, a spring damper system is incorporated into a translational joint located at the end of the tibia that represents the foot. A linear potentiometer provides a means of measuring the displacement of the spring that corresponds to a force feedback signal that can be used to compute stability criterion. A conceptual quadrupedal model with the designed legs is illustrated in Fig. 3.

IV. Kinematic Analysis

This section presents the kinematic analysis performed to estimate the foot position, using a multibody formulation. The configuration of the system can be determined by defining a vector of generalized coordinates $q_i = [r_i, \phi_i]^T$ for the position and orientation of each of the i links, where vector $r_i = [x_i, y_i]^T$ and ϕ_i denote the position and orientation, respectively of the i^{th} link center in the global frame. This frame is located at the hip joint as depicted by the revolute joint, D in Fig. 4 for our model. A multibody formulation is used to define the system's constraint equations, which in this case consists of the six revolute joints, along with a distance constraint between the hip joint, D and the driver joint, A and a driving constraint on the angular displacement of the driving link. The positions of the revolute joints are defined by specifying local position vectors, drawn from the i^{th} local frame to the adjacent revolute joints of each of the bodies. The revolute joint constraints can then be written as:

$$\Phi^{r(i,j)} = r_i + s_i^P - r_j - s_j^p = r_i + A_i s'^P_i - r_j - A_j s'^P_j = 0. \quad (1)$$

Here, A_i is the rotation matrix corresponding to a rotation by an angle ϕ_i about the global z-axis. The number of constraints is given by $T_c = 2n_r + 2d + d_r$, where n_r is the number of revolute joints, d is the number of distance constraints, and d_r is the number of driving constraints. Here, $n_r = 6$, $d_r = 1$, and $d = 1$, Hence $T_c = 15$.

Given estimations of the system's initial configuration, the Newton-Raphson method is used to solve for an initial position that is consistent with the constraints specified by Eq. (1). For the single-DOF mechanism, the crank angle is taken to be the driving input. Based on the value of the driving input, and the initial conditions of the system, the link positions may be computed iteratively as $x_f - x_0 = vt + \frac{1}{2}at^2$ for small time steps, where v and a are given by the velocity and acceleration equations at each time step, given by:

$$\dot{\mathbf{q}} = -\mathbf{\Phi}_\mathbf{q}^{-1}\mathbf{\Phi}_t \quad (2)$$

$$\ddot{\mathbf{q}} = -\mathbf{\Phi}_\mathbf{q}^{-1}\boldsymbol{\gamma} \quad (3)$$

Where γ is a vector of acceleration independent terms [23]. Here, $\mathbf{\Phi}_t \equiv v$ and $\mathbf{\Phi}_\mathbf{q}$ is the Jacobian. The generalized

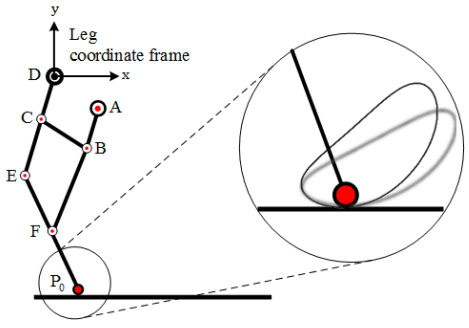

Fig. 4. Kinematic scheme adopted for the proposed mechanism. Here AB $=L_1$; BC $= L_2$; DE $= L_3$; BF $= L_4$; $EP_0=L_5$; DA $= L_6$. Shown in the inset are the trajectories generated. The light trajectory depicts one of the trajectories from the curve library discussed in sec. VI

positions calculated by the above multibody formulation are used to build a kinematic model to be able to track the foot trajectory of the leg throughout a full step cycle. The dark trajectory in Fig. 4 depicts the results of the kinematic simulation with heuristically selected link lengths. It can be observed that the trajectory follows a smooth curve. This demonstrates that this mechanism is capable of generating trajectories that minimize ground contact in order to maximize propulsive impulses. However, this trajectory shows that the initially selected parameters (position and orientation) require adjustments to generate a trajectory suitable for trotting.

While the simulated foot trajectory satisfies Requirement 3, further improvement of the link parameters is necessary to arrive at an angle of attack that is more conducive to forward propulsion. In order to reduce the size of the parametric design space, for future optimization, a sensitivity analysis was performed to determine the impact of key parameters on the resultant changes to the angle of attack.

V. Ideal Trajectory Generation

The workspace of single DOF legs is constrained by the design parameters (link lengths and configurations); thus, the foot trajectory cannot be altered once the designer determines these parameters. Therefore, optimization is required to trace a favorable trajectory also known as ideal trajectory. In this section, an effort to establish an ideal trajectory is undertaken.

For a dynamic gait such as trot, an ideal stance phase curve should be sinusoidal [24] while the swing-phase trajectory is an aspect of careful design. We establish a stance phase trajectory in order to make comparisons with the trajectories generated by the proposed mechanism discussed in Sec. VI. The swing-phase is modeled by a cubic spline using the Bezier curve [24] formulation, expressed as:

$$p_j(t) = \sum_{j=0}^{n} B_j^n(t) c_j \quad . \tag{4}$$

For $0 < t < 1$, where $c_j = \{c_0, c_1, \ldots, c_n\}$ is a set of control points defined to produce a specific curve and is the Bernstein basis polynomial of degree n. The control points are initially placed at the beginning, end and apex of the stance phase, and then iteratively weighted to arrive at the desired trajectory. The resulting trajectory should be smooth to avoid perturbations in the system during locomotion. The ideal stance-phase trajectory is as depicted in Fig. 5.

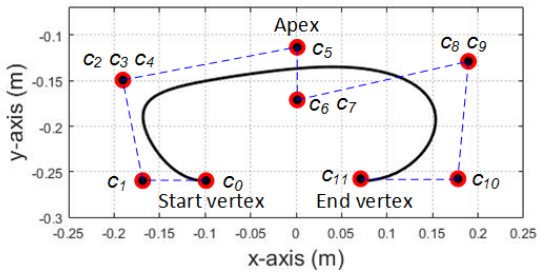

Fig.5. Plot depicting the ideal trajectory generated by Bezier curve formulation. The triple overlapping and double overlapping of control points increase the weight at that respective position and shapes the curve.

VI. Optimization

This section analyzes the effects of varying key link lengths on the foot trajectory, as part of the sensitivity analysis. Further, it establishes metrics to quantify the performance of simulated trajectories with respect to the ideal trajectory established in Sec. III.

A. Sensitivity Analysis

To address the challenge of optimizing the vast design space of a six-bar mechanism, preliminary optimization in terms of sensitivity analysis is performed. The result of this analysis is a condensed design space that is conducive to a rigorous optimization process. The kinematic model derived in Sec. IV is modified for the purpose of this analysis to accumulate multiple foot trajectories, their angle of attack, and their stride lengths, creating a library of simulations.

Varying position and orientation is a tedious process and one that requires much iteration. Furthermore, the Newton-Raphson method is a time consuming process due to the high-resolution requirements for convergence. We therefore apply the alternative approach of varying the link lengths themselves, thus varying position and orientation of the respective points defining the length. The design space of the lengths is given by the set $\{L_1, L_2, L_3, L_4, L_5, \text{and } L_6\}$. However, performing a brute-force sensitivity analysis on the complete design space is prohibitively computationally expensive. Instead, we identify two link lengths associated with the crank length, L_1 and the distance between the hip joint, located at point A, and the crank joint at point B, L_6. As L_1 is the driving link and L_6 dictates the position of the hip joint relative to the crank joint, these lengths are the most important driving factors of the foot trajectory shape and orientation and as such are the focus of the sensitivity analysis. The parameters for the analyses are varied within a sensible range, which are selected to ensure that the designed leg maintains a compact form factor that satisfies Requirement 5. The heuristically selected link lengths also dictate to what extent the lengths can be varied. Performing simulations beyond these bounds would result in singular configurations and end up adversely affecting the end trajectory to a point where smooth curves are no longer produced. These trajectories are in violation with Requirement 3 and as such are of no interest. The sensitivity analysis is undertaken with a focus on the effects of varying link lengths on angle of attack, α_0 and stride length due to their far-reaching effects on stability and distance traversed in one step-cycle.

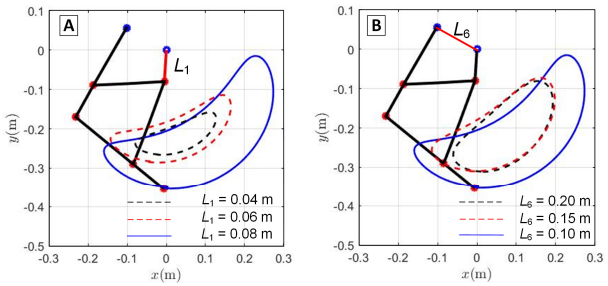

Fig.6. Bounded sensitivity analysis: (A) Crank shaft vs stride length (B) Hip-Crank distance vs Angle of attack.

First, L_1 is varied from 0.04 m to 0.08 m; the generated trajectories are stored and overlaid on each other as shown in Fig. 6(A). As shown, the generated trajectory at the upper limit has a shorter stride length in comparison to that generated by the lower bound. From the results produced, a preliminary conclusion is reached that increasing the length L_1 increases the stride length. To get a broader perspective of the effect of L_1 on the stride length and angle of affect, further simulation studies were conducted and plotted in Fig. 7. As shown, the preliminary conclusion is proven accurate from the plot. The driver link L_1 plotted on the left y-axis has a direct effect on the stride length. It is also evident from the same plot that the angle of attack is minimally affected, resulting in a leg position ahead of the symmetric axis on the hip, thus causing an imbalance during dynamic locomotion. It can be concluded that the longer the radius of the shaft, the longer the stride length. It is to be noted that varying the link L_1 beyond 0.08m showed irregular trajectories as mentioned earlier. Hence, for this set of heuristic link lengths, L_1 at 0.08m gives a maximum stride length while satisfying Requirements 3 and 5.

The sensitivity analysis on L_6 clarifies that varying the value of L_6 results in large changes to the orientation of the foot. From the geometry, we can infer that L_6 must be greater than L_1 or else the links will collide, while Requirement 5 can again bind the upper limits. For these simulations, the upper bound was selected to be 0.20 m and the lower bound to be 0.10 m, and simulations were performed between intervals of 0.05 m. The results of the simulation are illustrated in Fig. 6(B) and demonstrate that α_0 decreases with decrease in the length of L_6. Furthermore, to strengthen this observation, a series of simulation studies were performed. The second series of simulations were performed from 0.18 m to 0.06 m at an interval of 0.02 m. The result of this study, as shown in Fig. 7, reciprocates the results of first set of simulation done on L_6. It is worth noting from the same plot, the effect of L_6 on stride length is very small. These conclusions were not intuitive and were only established through the application of sensitivity analysis.

In conclusion, from these sensitivity analysis studies we learn that the stride length increases with the increase in the length L_1 and α_0 decreases with the decrease in length L_6. It is evident then, that in order to satisfy Requirement 4, the length L_6 must be small while remaining larger than L_1. There has to be a compromise of stride length to achieve an appropriate angle of attack.

B. *Curve Metrics*

In order to establish the best trajectory from the library of curves accumulated by sensitivity analysis, a qualitative comparison must be established. It is difficult for a single metric to estimate completely the similarities between two curves. Therefore, in this work, two parameters, the Hausdorff distance [25] and Jaccard distance [26] are employed to quantify the best possible trajectory. The first metric, the Hausdorff distance *H(A,B)*, calculates the Euclidean distance between the two sets of points, in this instance the desired trajectory established in Sec. V, and the trajectory being compared. It is expressed as:

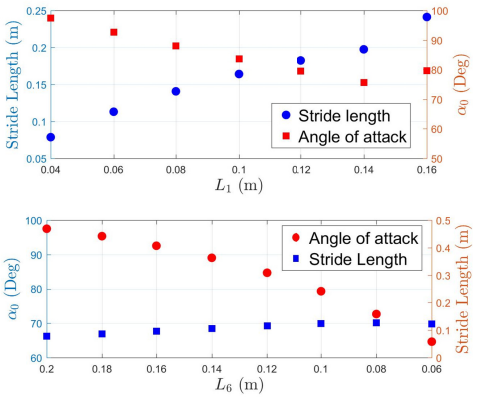

Fig.7. Plots showing the effects of varying link lengths L1 and L6 on angle of attack and stride length

$$H(A,B) = \max(h(A,B), h(B,A)) . \quad (5)$$

In (5), *h(A,B)* is the directed Hausdorff distance from set *A* to set *B*. From the generated library, smooth trajectories were selected, the Hausdorff distance was then computed, and the results are recorded in Table. I. As shown, the distance between the ideal and comparable trajectory is at a minimum for L_1 = 0.04 m and L_6 = 0.06 m, indicating that this particular curve among all the curves is closest to the ideal. However, this index does not consider the length or orientation of the curve; therefore we cannot discern from this metric any information on whether the indicated ideal is encompassing, encircled by, or tangent to the desired curve.

Another metric is therefore introduced to further quantize the generated trajectories. This metric compares the similarity of the two sets, A and B. and is known as Jaccard similarity index. It calculates the Jaccard distance d_J, which is a measure of the dis-similarity between the sets.

This can be established by first calculating the Jaccard index J_i, defined as:

$$J_i = \frac{A \cap B}{A \cup B} . \quad (6)$$

Further, $d_J = 1 - J_i$. The Jaccard distances are calculated for the same simulated trajectories as above and are shown in Table. II. The minimum value for d_J, 0.1148, corresponds to

TABLE I. HAUSDORFF DISTANCES OF THE SIMULATED TRAJECTORIES

Variables		H(A,B)	Variables		H(A,B)
L_1	L_6		L_1	L_6	
0.04	0.2	0.19	0.04	0.14	0.15
0.06	0.2	0.16	0.04	0.12	0.13
0.08	0.2	0.13	0.04	0.1	0.1
0.1	0.2	0.11	**0.04**	**0.06**	**0.084**

All units are in meters

TABLE II. JACCARD DISTANCES OF THE SIMULATED TRAJECTORIES

Variables		d_J	Variables		d_J
L_1	L_6		L_1	L_6	
0.04	0.2	0.1446	0.04	0.14	0.1352
0.06	0.2	0.1486	0.04	0.12	0.1278
0.08	0.2	0.1566	0.04	0.1	0.1234
0.1	0.2	0.1665	**0.04**	**0.06**	**0.1148**

All units are in meters

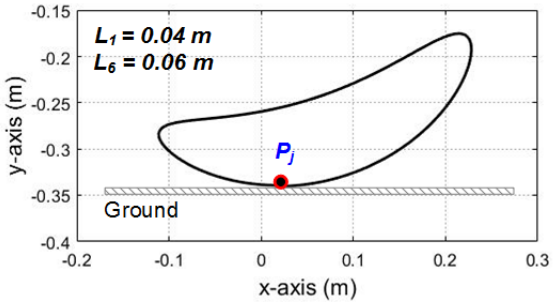

Fig.8. Realization of the best trajectory from the simulated trajectories

L_1 of 0.04 m and L_6 equal to 0.06 m. This indicates that curves generated by these parameters most closely resemble the ideal trajectory. This finding corroborates with the result obtained from Table. I. This trajectory, pictured in Fig. 8, is closest to the ideal of those contained within the curves generated by the selective optimization of link lengths L_1 and L_6. The angle of attack in this configuration, $\alpha_0 = 64.64°$, is in the range of stable running established in [22].

This result will be used as a starting point for rigorous optimization in future work to determine the remaining optimum design parameters.

VII. Conclusion

This paper presented a novel, single DOF leg mechanism in an effort to realize a dynamic gait while reducing mechanical and control complexity. A study is then conducted to identify crucial parameters of the design that affect the foot trajectory. Results of sensitivity analysis indicate that: (1) variations of crank radius proportionally affect the stride length, and (2) the variation of the distance between the hip and crank joint inversely affects the angle of attack. Moreover, with help of curve metrics, the trajectory closest to the designed ideal trajectory is identified.

Future work will include optimization of the dimensional parameters identified in Sec. VI.B to synthesize a gait that more closely generates the idealized swing-phase path. A leg prototype will be developed and its performance tested. Moreover, a quadruped integrating the proposed leg will serve as an experimental platform to study the performance enhancements that robotic tails provide.

Acknowledgment

The authors acknowledge the help of their colleagues, Peter Racioppo, William Rone, and Adam Williams.

References

[1] M. H. Raibert, "Trotting, pacing and bounding by a quadruped robot," *J. Biomech.*, vol. 23, no. SUPPL. 1, pp. 79–98, 1990.

[2] M. Hutter, C. Gehring, D. Jud, A. Lauber, C. D. Bellicoso, V. Tsounis, J. Hwangbo, P. Fankhauser, M. Bloesch, R. Diethelm, and S. Bachmann, "ANYmal - A Highly Mobile and Dynamic Quadrupedal Robot," *IEEE/RSJ IROS*, 2016.

[3] K. J. Waldron and R. B. McGhee, "The Adaptive Suspension Vehicle," *IEEE Control Syst. Mag.*, vol. 6, no. 6, pp. 7–12, 1986.

[4] R. J. Full, "Quantifying Dynamic Stability and Maneuverability in Legged Locomotion," *Integr. Comp. Biol.*, vol. 42, no. 1, pp. 149–157, 2002.

[5] H. Murao, H. Tamaki, and S. Kitamura, "Walking pattern acquisition for quadruped robot by using modular reinforcement learning," *2001 IEEE ICSMC*, vol. 3, no. 1, pp. 1402–1405.

[6] S.-M. Song and K. J. Waldron, *Machines That Walk*. MIT Press, 1988.

[7] W. Saab and P. Ben-Tzvi, "Design and Analysis of a Robotic Modular Leg Mechanism," in *ASME IDETC/CIE*, pp. 1–8, 2016.

[8] W. S. Rone and P. Ben-Tzvi, "Static Modeling of a Multi-Segment Serpentine Robotic Tail," in ASME *IDETC/CIE*, pp. 1–9, 2015.

[9] W. S. Rone and P. Ben-Tzvi, "Continuum Robotic Tail Loading Analysis for Mobile Robot Stabilization and Maneuvering," in *ASME IDETC/CIE*, 2014, vol. 1, pp. 1–8.

[10] W. Rone and P. Ben-Tzvi, "Dynamic Modeling and Simulation of a Yaw-Angle Quadruped Maneuvering With a Planar Robotic Tail," *J. Dyn. Syst. Meas. Control*, vol. 138, no. 8, p. 84502, 2016.

[11] W. S. Rone and P. Ben-Tzvi, "Multi-Segment Continuum Robot Shape Estimation Using Passive Cable Displacements," *IEEE Int. Symp. Robot. Sensors Environ.*, no. 1334227, pp. 21–23, 2013.

[12] R. M. Alexander, "The Gaits of Bipedal and Quadrupedal Animals," *Int. J. Rob. Res.*, vol. 3, no. 2, pp. 49–59, 1984.

[13] A. Wang, S. Seok, A. Wang, D. Otten, and S. Kim, "Actuator Design for High Force Proprioceptive Control in Fast Legged Locomotion Actuator Design for High Force Proprioceptive Control in Fast Legged Locomotion," no. February 2016, pp. 1970–1975, 2012.

[14] D. Jin Hyun, S. Seok, J. Lee, and S. Kim, "High speed trot-running: Implementation of a hierarchical controller using proprioceptive impedance control on the MIT Cheetah," *Int. J. Rob. Res.*, vol. 33, no. 11, pp. 1417–1445, 2014.

[15] C. Semini, N. G. Tsagarakis, E. Guglielmino, M. Focchi, F. Cannella, and D. G. Caldwell, "Design of HyQ - a hydraulically and electrically actuated quadruped robot," *Proc. Inst. Mech. Eng. Part I J. Syst. Control Eng.*, vol. 225, no. 6, pp. 831–849, 2011.

[16] H. Khan, S. Kitano, M. Frigerio, M. Camurri, V. Barasuol, R. Featherstone, D. G. Caldwell, and C. Semini, "Development of the lightweight hydraulic quadruped robot - MiniHyQ," *IEEE Conf. Technol. Pract. Robot Appl. TePRA*, vol. 2015–Augus, 2015.

[17] J. Park, K.-S. Kim, and S. Kim, "Design of a cat-inspired robotic leg for fast running," *Adv. Robot.*, vol. 28, no. 23, pp. 1587–1598, 2014.

[18] U. Saranli, M. Buehler, and D. E. Koditschek, "RHex: A Simple and Highly Mobile Hexapod Robot," *Int. J. Rob. Res.*, vol. 20, no. July, pp. 616–631, 2001.

[19] C. Tavolieri, E. Ottaviano, M. Ceccarelli, and A. Di Rienzo, "Analysis and Design of a 1-DOF Leg for Walking Machines," *15th Int. Work. Robot. AlpeAdria-Danube Reg. Balantonfured, CD Proceedings,* 2006.

[20] A. Ghassaei, P. P. Choi, and D. Whitaker, "The Design and Optimization of a Crank-Based Leg Mechanism," 2011.

[21] A. Seyfarth, H. Geyer, and H. Herr, "Swing-leg retraction: a simple control model for stable running.," *J. Exp. Biol.*, vol. 206, no. Pt 15, pp. 2547–2555, 2003.

[22] H. Geyer, A. Seyfarth, and R. Blickhan, "Spring-mass running: Simple approximate solution and application to gait stability," *J. Theor. Biol.*, vol. 232, no. 3, pp. 315–328, 2005.

[23] E. . Haug, "Intermediate Dynamics," Prentice Hall College Div, 1991, p. pp 48-108.

[24] D. J. Hyun, J. Lee, S. Park, and S. Kim, "Implementation of trot-to-gallop transition and subsequent gallop on the MIT Cheetah I," *Int. J. Robot. Res.*, pp. 1–24, 2016.

[25] D. P. Huttenlocher, G. A. Klanderman, and W. J. Rucklidge, "Comparing Images Using the Hausdorff Distance," *IEEE Trans. Pattern Anal. Mach. Intell.*, vol. 15, no. 9, pp. 850–863, 1993.

[26] S. Niwattanakul, J. Singthongchai, E. Naenudorn, and S. Wanapu, "Using of Jaccard Coefficient for Keywords Similarity," *Int. MultiConference Eng. Comput. Sci.*, vol. I, pp. 380–384, 2013.

[27] J. E. Mckenzie, "Design of Robotic Quadruped Legs," 2012.

[28] C. Semini, "HyQ - Design and Development of a Hydraulically Actuated Quadruped Robot," *Darwin*, no. April, p. 210, 2010.

[29] "CHEETAH - Fastest Legged Robot." [Online]. Available: http://www.bostondynamics.com/robot_cheetah.html. [Accessed: 09-Feb-2017].